Proceedings of the IASS 2024 Symposium
Redefining the Art of Structural Design
August 26-30, 2024, Zurich, Switzerland
Philippe Block, Giulia Boller, Catherine DeWolf,
Jacqueline Pauli, Walter Kaufmann (eds.)

Improved Multibody Rope Approach for Free-Form Gridshells Shape and Construction

Amedeo MANUELLO BERTETTO[*], Jonathan MELCHIORRE [a], Giuseppe Carlo MARANO[a]

[*] Department of Structural, Geotechnical and Building Engineering Politecnico di Torino
amedeo.manuellobertetto@polito.it
[a] Department of Structural, Geotechnical and Building Engineering Politecnico di Torino

Abstract

Because gridshell roofing design may be used to build large, lightweight roofs with slender primary structural parts, in today's engineering and architecture, they are appearing increasingly frequently. However, their extended use outside of the most expensive and emblematic buildings or belonging to great architecture has been limited by their difficulty in realization and expensive in production phase. Since the stress state and structural form of gridshells are closely related, it is important to choose the optimal design configuration to reduce internal stresses. Multi-body Rope Approach (MRA) computing d'Alembert's principle guaranteed equilibrium for every node of a funicular system in a dynamic model of falling bodies over sequential steps in the time domain, returning a final funicular configuration. Different MRA improving methodologies are proposed in this paper: Repulsive Nodes MRA (RN-MRA) and Multiple Order MRA (MO-MRA). By combining these methods, an enhanced MRA (i-MRA) is created that significantly reduces the variety of structural components needed for gridshell fabrication. Furthermore, the suggested approach provides lower manufacturing costs and improves building stage management efficiency. Finally, by putting the i-MRA to use in Matlab and evaluating it in a case study, its efficacy was confirmed.

Keywords: Gridshell, Multi-body Rope Approach, Structural Efficiency, optimization, Improved MRA, Form-finding)

1. Introduction: Multi-body Rope Approach

In recent years, advancements in digital design and fabrication technologies have expanded the possibilities for gridshells design and construction. These structures, constituted by materials like steel (e.g., [1]), aluminium (e.g., [2]), wood (e.g., [3, 4, 5, 6]), and elastic composite materials (e.g., [7, 8, 9]), have seen increased use. However, their construction still faces challenges due to geometric complexity and building phases (e.g., [10]). Nonetheless, improvements in computing systems have enhanced the ability to analyze and compute complex systems (e.g., [11]). Consequently, it is possible to anticipate continued growth in the utilization of gridshells for designing and constructing large, open structures in the coming years. For these structures, the force density method is one of the most widely used form-finding techniques [12] together with the thrust network analysis [13], the dynamic relaxation method [14], the particle-spring system [15], the multi-body rope approach [16, 17, 18], and others [19, 20]. A cutting-edge development in structural design research is the combination of free shapes and free-form structures with structural optimization. The necessity to reduce the number of different element types in gridshell construction is equally a topical issue[21, 22, 23]. Determining a structural model that is both geometrically and structurally optimal is substantially difficult. This work presents a novel improvement in form-finding techniques designed especially for gridshells: the improved Multi-body

Rope Method (i-MRA). The i-MRA method built upon the Multi-body Rope Approach (MRA) [16], is a form-finding method used in structural engineering to maximize the number of parts of identical length while designing complex and free-form gridshells.

The Multibody Rope Approach (MRA), developed by Manuello [16] and originally presented in 2004, presents a novel method for producing gridshell structures even with complex geometries and varying forming loads reducing the number of unequal elements as much as possible. This technique is designed for gridshell buildings that use standardized building materials and free-form designs. MRA uses a dynamic model that represents falling bodies in both space and time. D'Alembert's principle is employed to define the most reliable setup for every node repeatedly. This method presentation of structural components as useful ropes joining masses to nodes is one of its distinguishing features. The goal is to produce a geometry with the maximum number of components of the same length and the best structural performance. The final equilibrium configuration is a funicular configuration, which is an inverted depiction of the hanging net. MRA makes the same assumption as particle-spring models: that rope loads and nodes self-weight are localized at the nodes. However, MRA departs from previous approaches by modelling the hanging network with ropes and adding a certain slack coefficient to handle regular shapes. The forces operating on individual nodes in MRA are not the same as those in dynamic relaxation (DR) and spring-particle (SP) techniques. Interestingly, the rope element exerts pulls on the masses to keep them from travelling farther than the given distance a distance that exactly matches the rope length (l_{rope}). The forces F applied to the end nodes may be expressed as follows defining l as the distance between the rope two ends and k as the rope axial stiffness:

$$\begin{cases} F_{rope} = 0 & \text{if} \quad l < l_{rope} \\ F_{rope} = k(l - l_{rope}) & \text{if} \quad l \geq l_{rope} \end{cases} \tag{1}$$

In general, the goal of the method is to find a geometric configuration that ensures that the nodes remain in balance both from external forces and those generated by the ropes that connect them. Let's examine a typical node i with a mass of m_i within the network of nodes and ropes. Node i is linked to a quantity n_i of other nodes through ropes. If there exists an external load p_i applied to node i, the equilibrium equation can be formulated as:

$$\vec{R}_i = \vec{p}_i + \sum_{j=1}^{n_i} \vec{F}_{rope,ji} + \vec{F}_i^I + \vec{F}_i^{II} = 0 \tag{2}$$

The force on node i in this equation is represented by the vector $\vec{R}i$, which consists of many forces: the external load p_i, the forces that the ropes transfer $\vec{F}$rope, ji, the inertial force $\vec{F}_i^{II}$, and the damping force $\vec{F}_i^I$. The node mass m_i and the acceleration vector magnitude $\vec{a}_i$ are multiplied to determine the magnitude of the inertial force $\vec{F}_i^{II}$, with the inertial force direction being opposite to that of the node acceleration. A constant damping coefficient c_i and the velocity vector $\vec{v}_i$ are multiplied to find the damping force $\vec{F}_i^I$, which is oriented in the opposite direction of the velocity vector. By representing the position of the generic node i as $\vec{u}_i = (x_i, y_i, z_i)$, it is possible to derive the velocity and acceleration by differentiating the position with respect to time, as outlined in equations (3).

$$\vec{v}_i = \dot{\vec{u}}_i = (\dot{x}_i, \dot{y}_i, \dot{z}_i) \qquad \vec{a}_i = \ddot{\vec{u}}_i = (\ddot{x}_i, \ddot{y}_i, \ddot{z}_i) \tag{3}$$

Therefore, equation (2) can be reformulated as shown in (4).

$$\vec{R}_i = \vec{p}_i + \sum_{j=1}^{n_i} \left\{ k \cdot \vec{F}_{rope,ji} \right\} - c_i \cdot \vec{v}_i - m_i \cdot \vec{a}_i = 0 \tag{4}$$

A time step of Δt is taken into consideration in order to solve the system of equations. With initial velocities and accelerations set to zero for each node i ($v_i(0) = 0$ and $a_i(0) = 0$), the locations of the nodes at time $t = 0$ are taken to be known. Each node location, velocity, and acceleration at time t may be used to calculate these values at the following time step, $t + \Delta t$. Equation (5) illustrates how a coefficient C_3 is defined as a function of the known node locations at time t^* in order to achieve this.

$$C_3 = \vec{p}_i + \sum_{j=1}^{n_i} \left\{ k \cdot \vec{F}_{rope,ji} \right\} \tag{5}$$

The coefficient C_3 relies entirely on the node positions at time t^*, and it determines the vector F_{rope}. Thus, Equation (4) can be revised as depicted in (6).

$$\ddot{\vec{u}} + \frac{c}{m}\dot{\vec{u}} = C_3 \tag{6}$$

Furthermore, the natural frequency of the system ω_n and the critical damping ζ can be characterized by equations (7) and (8) respectively.

$$\omega_n = \sqrt{\frac{k}{m}} \tag{7}$$

$$\zeta = \frac{c}{2\omega_n m} \tag{8}$$

The external force term $F_{\text{text}}(t)$ makes this second-order differential equation non-homogeneous. The stiffness, mass, and damping coefficient of the system are denoted by the constants k, m, and c, respectively. The frequency at which the system oscillates in the absence of outside influences is known as the natural frequency, or ω_n. Conversely, the damping coefficient that causes the system to be critically damped—that is, to return as quickly as feasible to its equilibrium state without oscillating—is known as the critical damping ζ.

$$\ddot{\vec{u}} + 2\omega_n\zeta\dot{\vec{u}} = C_3 \tag{9}$$

The solution to equation (9) can be derived by combining the particular solution with the solution to the corresponding homogeneous differential equation, represented by (10).

$$\vec{u}(t) = C_1 e^{-2\omega_n\zeta} + C_2 + \frac{C_3}{2\omega_n\zeta}t \tag{10}$$

The system starting conditions may be used to get the coefficients C_1 and C_2. In this case, The positions and velocities of the nodes at the time step may be used to compute them $t - \Delta t$ that came right before, as shown in the following equations:

$$C_1 = -\frac{2\omega_n\zeta\dot{\vec{u}}_{(t-\Delta t)} - C_3}{(2\omega_n\zeta)^2} \tag{11}$$

$$C_2 = -\frac{(2\omega_n\zeta)^2\vec{u}_{(t-\Delta t)} + 2\omega_n\zeta\dot{\vec{u}}_{(t-\Delta t)} - C_3}{(2\omega_n\zeta)^2} \tag{12}$$

The locations, velocities, and accelerations of the system nodes at the previous time instant in the solution determine the values of the coefficients C_1, C_2, and C_3. Gradually, the positions of the nodes at each instant may be calculated, starting with the initial condition when the location of the node is known and their acceleration and velocity are zero. By calculating the difference between the nodes locations at instants $t - \Delta t$ and t, and dividing by the time increment Δt, one may derive the velocity vector $\dot{\vec{u}}_t$:

$$\dot{\vec{u}}_t = \frac{\vec{u}_t - \vec{u}_{t-\Delta t}}{\Delta t} \tag{13}$$

The ratio of the incremental change in velocity between two time instants may be calculated $t - \Delta t$ and t to find the acceleration $\ddot{\vec{u}}_t$. This entails calculating and dividing the velocity difference between these two points in time by Δt.

$$\ddot{\vec{u}}_t = \frac{\dot{\vec{u}}_t - \dot{\vec{u}}_{t-\Delta t}}{\Delta t} \tag{14}$$

The proposed method aims at identifying the final shape of a gridshell starting from its original mesh, which is the state of the net at the beginning (mesh on the flat). When the initial node positions are known and taken to belonging to the z=0 plan, the following equations are used to compute the new node locations, velocities, and accelerations in turn: (10), (13), and (14). This repeating approach is performed $\vec{p}$ until the applied force field-given optimal structural geometry is reflected in an equilibrium configuration. The final geometry is affected by nodal masses m, system stiffness k, damping parameters c, rope slack coefficient ρ, and the applied force field $\vec{p}$. The slack coefficient ρ is defined as the ratio between the desired length of the ropes (l_{rope}) respect to the initial distance between the nodes, as specified in the equation (15).

$$\rho_{ij} = \frac{l_{rope}}{|\vec{u}_i(0) - \vec{u}_j(0)|} \tag{15}$$

Two enhanced variants of MRA, Repulsive Nodes MRA (RN-MRA) and Multiple Orders MRA (MO-MRA), are presented in this study with the goal of lowering the quantity of "loose elements" produced by MRA. The loose elements are the ropes remained loose, not in tension after the form-finding. These techniques can be used after MRA to improve the final arrangement, leading to a structure with fewer parts of different lengths and making the assembly to be easier. The combination of these methods is known as Improved MRA (i-MRA), which may produce structurally efficient and easily buildable and constructible geometries by carefully choosing model parameters and target lengths.

2. Improved MRA: Multiple Orders and Repulsive nodes

The Multiple Order MRA (MO-MRA) technique aims to decrease the number of distinct structural elements obtained from traditional MRA. The structural layout derived from applying MRA typically consists of structural elements of length $l_{\text{rope},1}$ along with additional "loose elements." MO-MRA involves introducing new sets of ropes, each characterized by a length shorter than $l_{\text{rope},1}$.

For each iteration, the assignment of ropes to these sets is determined based on the distance between the connected nodes. Once the geometric configuration is obtained using MRA, a new set of ropes with a final length of $l_{\text{rope},2} < l_{\text{rope},1}$ is added. In this scenario, the force $\vec{F}$rope exerted by each rope depends on

its assigned set, which is determined by the distance between the connected nodes. Specifically, $\vec{F}$rope can be computed as described in equation (16).

$$\begin{cases} F_{rope} = 0 & \text{if} \quad l < l_{rope,2} \\ F_{rope} = k(l - l_{rope,2}) & \text{if} \quad l_{rope,2} < l \leq \gamma(l_{rope,1} - l_{rope,2}) + l_{rope,2} \\ F_{rope} = 0 & \text{if} \quad \gamma(l_{rope,1} - l_{rope,2}) + l_{rope,2} < l < l_{rope,1} \\ F_{rope} = k(l - l_{rope,1}) & \text{if} \quad l \geq l_{rope,1} \end{cases} \tag{16}$$

The resulting equilibrium configuration is iteratively determined using equations (10), (13), and (14), resulting in a new structural arrangement. In this updated setup, structural elements are categorized into three groups: those with target lengths $l_{\text{rope},1}$ and $l_{\text{rope},2}$, and possibly a third group comprising "loose elements."

Once more sets of ropes have been added, the repetition of this procedure should be performed until all structural components have been classified into distinct groups. By combining structural elements of comparable lengths, this technique expedites the building of gridshells and facilitates mass manufacturing while streamlining on-site strategy.

MO-MRA provides users with the flexibility to adjust parameters such as the coefficient γ and rope lengths ($l_{\text{rope},2}$, $l_{\text{rope},3}$, etc.) to customize the structural geometry to suit their design requirements. These parameters are customizable and enable optimization of the structural design to meet specific construction or manufacturing limitations. For example, while $l_{\text{rope},1}$ may dictate the structure height, it could lead to material waste when cutting steel billets of fixed length. Thus, adjusting the lengths of other structural element families can help minimize waste.

Similarly, the coefficient γ determines the allocation of slack ropes, remaining after MRA application, to different structural element families. Configuring both γ and the target lengths for each family is crucial in defining the final structural geometry, which can vary widely based on project-specific requirements.

The Repulsive Nodes MRA is devised to decrease the number of "loose elements" produced by applying basic MRA. The fundamental concept involves introducing a repulsive force field $\vec{q}$ among the nodes of the geometric configuration obtained through MRA. This force field $\vec{q}$ is implemented after establishing the final equilibrium configuration using MRA, necessitating a new iterative computation process to determine the updated equilibrium condition.

Until the ropes are tensioned, repulsion will occur because the repulsive forces operate on the ends of each slack rope, causing the linked nodes to move apart as if they were electrically charged with the same polarity. Therefore, for every node linked by a loose rope, Equation (4) must be adjusted to incorporate the repulsive force field $\vec{q}$. Consequently, a new system of equations is derived, where Equation (4) remains applicable for nodes linked by tensioned ropes, and Equation (17) is introduced for each node i connected to slack rope.

$$\vec{R}_i = \vec{p}_i + \vec{q}_i + \sum_{j=1}^{n_i} \left\{ k \cdot \vec{F}_{rope,ji} \right\} - c_i \cdot \vec{v}_i - m_i \cdot \vec{a}_i = 0 \tag{17}$$

Equation (17) introduces a repulsive force field $\vec{q}$ to each node i connected by slack ropes. This force, $\vec{q}$, is directly proportional to the disparity between the target length l_{rope} and the distance l_{ij} between nodes linked by a slack rope. To compute the repulsive force field $\vec{q}$, Equation (18) can be applied, with k_{rep} representing the constant of proportionality relating the magnitude of the repulsive force to the distance between nodes i and j.

$$q_i = -k_{rep}(l_{rope} - l_{ij}) \tag{18}$$

The choice of elastic coefficients k and k_{rep} depends on various factors. For instance, k should be determined based on rope length, applied loads, nodal masses, and the time interval Δt for each iteration. It needs to be sufficiently large to prevent the presence of "over elements" yet not too large to ensure system convergence. In the reported application cases, a k value of $1.2, \text{MN/m}$ with $\Delta t = 0.005, \text{s}$ was utilized, serving as a starting point for different scenarios. The procedure involves increasing k until no more "over elements" are present in the final configuration and adjusting Δt if the system fails to converge. Similarly, k_{rep} should be chosen to prevent repulsive forces between nodes from generating "over elements" in the final geometric configuration. In the presented case studies, a k_{rep} of $2, \text{kN/m}$ was employed, serving as an initial value for other applications. Therefore, it is advisable to apply RN-MRA judiciously, making minor adjustments to the geometry obtained from MO-MRA to strike a balance between enhancing constructability and achieving the best structural geometry. Ideally, RN-MRA should be used for models with few "loose elements" relative to tensioned ones, and where their length closely aligns with the target length l_{rope}.

Two MRA breakthroughs that result in more beneficial structural solutions in terms of ease of construction are addressed in this Section. These methods are used in the i-MRA process to provide a geometry that strikes the ideal mix of structural functionality and simplicity of assembly. In the first method, the number of element families in the MO-MRA is increased until a configuration is reached where the majority of the ropes are in tension. The remaining loose parts are subsequently tensioned using the second method, RN-MRA, to enhance the geometry. Because of this, the final form may not exactly match the geometry produced by MO-MRA alone, but it is distinguished by the least amount of *loose elements*.

3. Free-form Geometry

The purpose of the case study is to evaluate the suggested method efficacy in a wide range of scenarios. Applying the technique to a base plan with a free-form curve such that its definition entails having parametric design software create the mesh automatically. The two types of meshes that are the focus of the investigation are a quadrangular mesh and a mesh made up of hexagonal and pentagonal pieces. The edges in this Section of two meshes have an average length of about 1.50 meters. However, there is a large degree of diversity in the initial elements due to the length range of the quadrangular mesh constituent parts, which is around 0.80m to 2.30m. For the quadrangular mesh scenario, the structural configuration produced using basic MRA with $\rho_{avg} = 1.20$ is shown in Figures 1a and 1c. In this instance, structural parts that end up longer than the desired length of $L_{rope} = 1.78m$ (*loose ropes*) are shown in red. Because of the changes in the initial geometry, these elements make up more than 13% of the 750 structural pieces that constitute the gridshell. As a result, building a real structure calls for more than a hundred distinct kinds of structural components. Although this might be handled on the job site, it presents difficulties for complicated and general structural shapes, making the administration of the building process more difficult.

However, the structural configuration achieved through the application of i-MRA, as presented in this paper, is depicted in Figures 1b and 1d. The improvement realized in this scenario is remarkable. This technique enabled the calculation of a structural geometry that can be executed using only 7 types of structural components with lengths $L_{rope} = [1.78; 1.58; 1.45; 1.35; 1.25; 1.15]m$. This outcome is impressive and underscores how the methodologies outlined in Section 1. can significantly simplify construction complexity.

The results of the structural analyses presented in Figure 2 show that the structural geometry changes

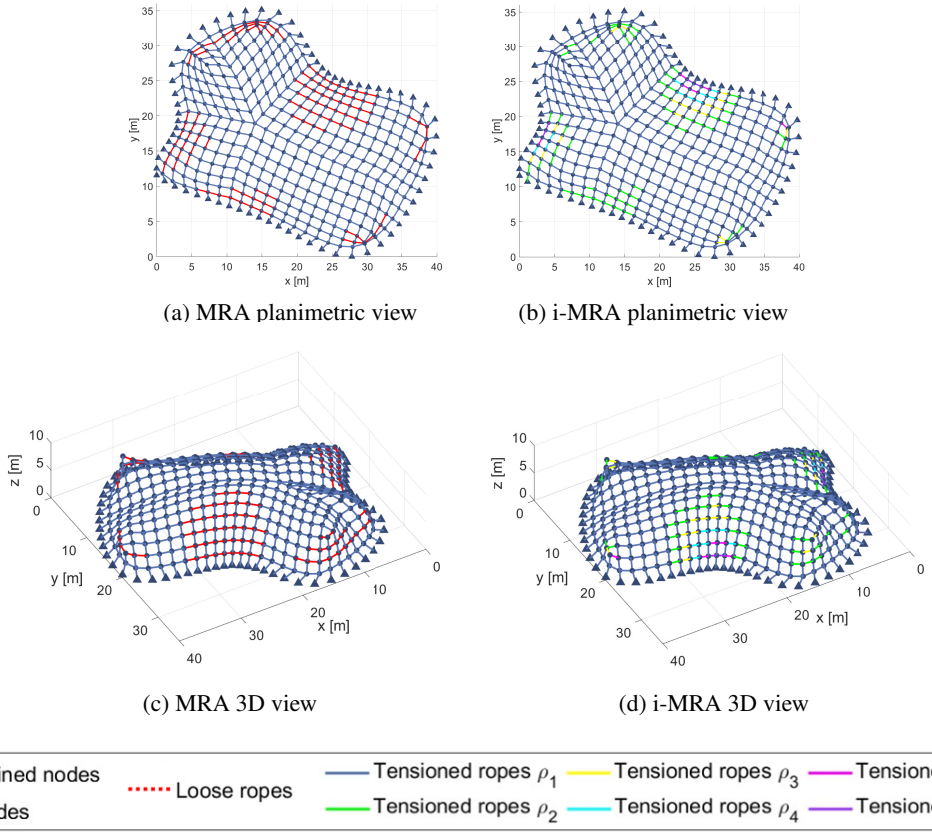

(a) MRA planimetric view (b) i-MRA planimetric view

(c) MRA 3D view (d) i-MRA 3D view

Figure 1: MRA and i-MRA comparison using quadrangular mesh on a free-form structure. All the blue ropes present the same length, the red ones are the loose elements

made possible by i-MRA do not cause a noticeably higher level of stress. When compared to the fundamental form-finding geometry (on the left), the structure calculated using i-MRA (on the right) shows comparable values of axial force and bending moment. By using i-MRA, the number of structural components used decreased from over 100 to just 6. Less than 0.7 % was a minor rise in the Von Mises stresses despite the imposed geometric alterations. In addition, there was a roughly 20-fold reduction in construction complexity as determined by the range of structural element types used.

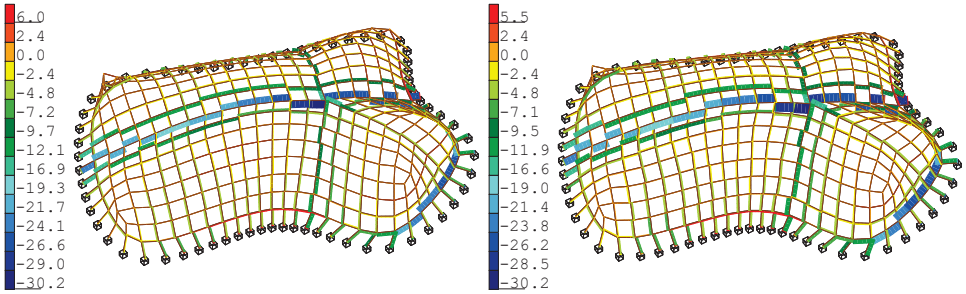

(a) MRA: $|N|_{max} = 6.0kN$ (b) i-MRA: $|N|_{max} = 5.5kN$

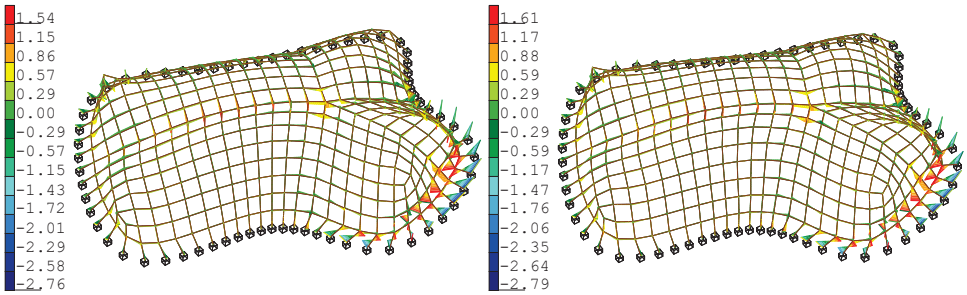

(c) MRA: $|M|_{max} = 2.76kNm$ (d) i-MRA: $|M|_{max} = 2.79kNm$

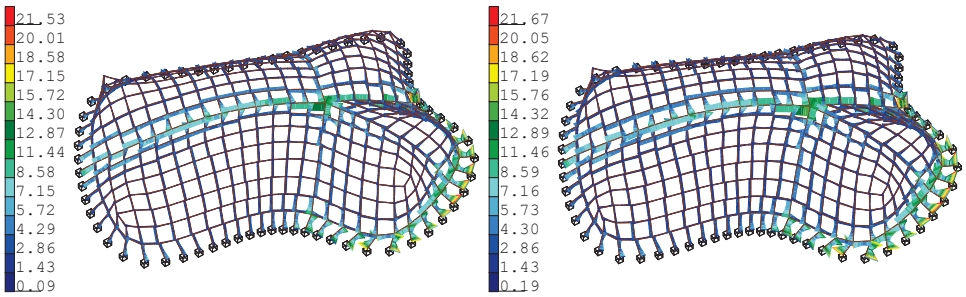

(e) MRA: $|\sigma^{VM}|_{max} = 21.53kPa$ (f) i-MRA: $|\sigma^{VM}|_{max} = 21.67kPa$

Figure 2: Structural analysis of the structure with quadrangular mesh using basic MRA (left) and i-MRA (right). Comparison between Von Mises stress (kPa) (bottom), bending moment (kNm) (middle), and axial force (kN) (top). The assumed load is the structure's own weight, and the material used is steel.

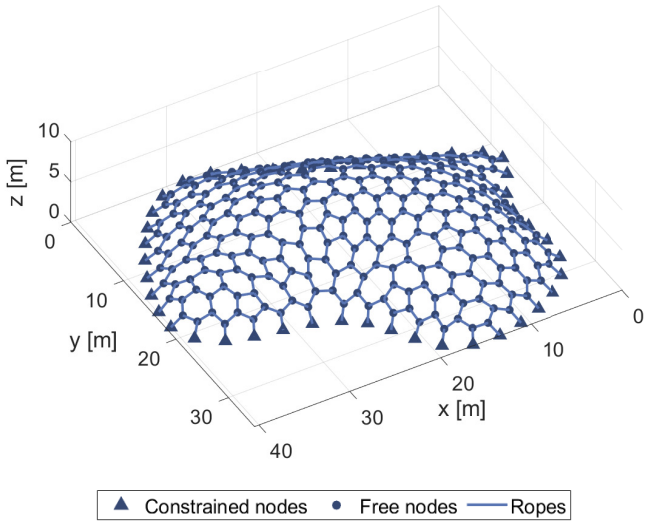

Figure 3: MRA implementation on a hexagonal mesh free-form structure with $\rho = 1.10$.

4. Conclusions

The paper introduces improvements for a form-finding method for gridshell structures originally proposed by the authors. Once a load condition is set, the basic MRA defines a structural geometry with minimized eccentricity of compression forces, reducing bending moments. This approach models the structure as masses connected by loose ropes, with dynamics solving yielding an equilibrium configuration. To simplify construction management and reduce computational effort, two enhancement methods are proposed for the basic MRA. The first involves grouping elements with identical lengths to minimize required structural element types. The second introduces a repulsive force field to adjust geometry, reducing unmatched components. The combination, termed i-MRA, is effective. Testing in an example of free-form gridshell i-MRA shows a significant reduction in required components, especially with complex geometry. Structural analysis indicates a minimal impact on static behaviour, with negligible increases in internal actions and stress. Results also show the base mesh has minimal influence on slack coefficient trends, while the initial mesh significantly affects the final geometry. This research lays the groundwork for further exploration, including assessing method impacts on structural performance and instability, integrating into optimization procedures, and optimizing panel and node shapes.

References

[1] W. Sobek and L. Blandini, "The mansueto library–notes on a glazed steel grid shell from design to construction," in *Challenging Glass Conference Proceedings*, vol. 2, 2010, pp. 179–186.

[2] C. Zhao, J. Ma, S. Du, Y. Gu, and Y. Zhou, "Mechanical properties of a novel joint of a single-layer aluminum-alloy combined lattice-shell structure," *Mater. Tehnol*, vol. 53, pp. 811–819, 2019.

[3] E. Happold and L. WI, "Timber lattice roof for the mannheim bundesgartenschau," 1975.

[4] R. Harris, "Design of timber gridded shell structures," *Proceedings of the Institution of Civil Engineers-Structures and Buildings*, vol. 164, no. 2, pp. 105–116, 2011.

[5] M. Collins and T. Cosgrove, "A review of the state of the art of timber gridshell design and construction," 2016.

[6] J. Chilton and G. Tang, *Timber gridshells: architecture, structure and craft*. Routledge, 2016.

[7] C. Douthe, J.-F. Caron, and O. Baverel, "Gridshell structures in glass fibre reinforced polymers," *Construction and building materials*, vol. 24, no. 9, pp. 1580–1589, 2010.

[8] O. Baverel, J.-F. Caron, F. Tayeb, and L. Du Peloux, "Gridshells in composite materials: Construction of a 300 m2 forum for the solidays' festival in paris," *Structural engineering international*, vol. 22, no. 3, pp. 408–414, 2012.

[9] B. D'Amico, A. Kermani, H. Zhang, A. Pugnale, S. Colabella, and S. Pone, "Timber gridshells: Numerical simulation, design and construction of a full scale structure," in *Structures*, Elsevier, vol. 3, 2015, pp. 227–235.

[10] E. L. Hernández, O. Baverel, and C. Gengnagel, "On the design and construction of elastic gridshells with irregular meshes," *International Journal of Space Structures*, vol. 28, no. 3-4, pp. 161–174, 2013.

[11] S. H. Dyvik, B. Manum, and A. Rønnquist, "Gridshells in recent research—a systematic mapping study," *Applied Sciences*, vol. 11, no. 24, p. 11 731, 2021.

[12] H.-J. Schek, "The force density method for form finding and computation of general networks," *Computer methods in applied mechanics and engineering*, vol. 3, no. 1, pp. 115–134, 1974.

[13] J. R. H. Otter, A. C. Cassell, R. E. Hobbs, and POISSON, "Dynamic relaxation," *Proceedings of the Institution of Civil Engineers*, vol. 35, no. 4, pp. 633–656, 1966.

[14] P. Block and J. Ochsendorf, "Thrust network analysis: A new methodology for three-dimensional equilibrium," *Journal of the International Association for shell and spatial structures*, vol. 48, no. 3, pp. 167–173, 2007.

[15] A. Kilian and J. Ochsendorf, "Particle-spring systems for structural form finding," *Journal of the international association for shell and spatial structures*, vol. 46, no. 2, pp. 77–84, 2005.

[16] A. Manuello, "Multi-body rope approach for grid shells: Form-finding and imperfection sensitivity," *Engineering Structures*, vol. 221, p. 111 029, 2020.

[17] J. Melchiorre, A. Manuello Bertetto, F. Marmo, S. Adriaenssens, and G. C. Marano, "Gdifferential formulation and numerical solution for elastic arches with variable curvature and tapered cross-sections," in *European Journal of Mechanics-A/Solids*, ScienceDirect, 2023, pp. 97, 104757.

[18] J. Melchiorre, S. Soutiropoulos, A. Manuello, G. C. Marano, and F. Marmo, "Grid-shell multi-step structural optimization with improved multi-body rope approach and multi-objective genetic algorithm," in *Shell and Spatial Structures*, Springer, 2023.

[19] I. M. Rian, M. Sassone, and S. Asayama, "From fractal geometry to architecture: Designing a grid-shell-like structure using the takagi–landsberg surface," *Computer-Aided Design*, vol. 98, pp. 40–53, 2018.

[20] W. Huang, C. Wu, J. Hu, and W. Gao, "Weaving structure: A bending-active gridshell for freeform fabrication," *Automation in Construction*, vol. 136, p. 104 184, 2022.

[21] K. Yamamoto *et al.*, "State-of-the-art for optimization of forms and strength for reticulated shells," in *IASS Annual Symposium; IASS-APCS: London, UK*, 2012.

[22] S. Adriaenssens, P. Block, D. Veenendaal, and C. Williams, *Shell structures for architecture: form finding and optimization*. Routledge, 2014.

[23] L. Bouhaya, O. Baverel, and J.-F. Caron, "Optimization of gridshell bar orientation using a simplified genetic approach," *Structural and Multidisciplinary Optimization*, vol. 50, pp. 839–848, 2014.